

Referenceless Interleaved Echo-Planar Imaging

Scott B. Reeder,¹ Ergin Atalar,^{2*} Anthony Z. Faranesh,¹ and Elliot R. McVeigh^{1,2}

Interleaved echo-planar imaging (EPI) is an ultrafast imaging technique important for applications that require high time resolution or short total acquisition times. Unfortunately, EPI is prone to significant ghosting artifacts, resulting primarily from system time delays that cause data matrix misregistration. In this work, it is shown mathematically and experimentally that system time delays are orientation dependent, resulting from anisotropic physical gradient delays. This analysis characterizes the behavior of time delays in oblique coordinates, and a new ghosting artifact caused by anisotropic delays is described. "Compensation blips" are proposed for time delay correction. These blips are shown to remove the effects of anisotropic gradient delays, eliminating the need for repeated reference scans and postprocessing corrections. Examples of phantom and in vivo images are shown. *Magn Reson Med* 41:87–94, 1999. © 1999 Wiley-Liss, Inc.

Key words: MRI; EPI; reconstruction; calibration; reference scans; compensation blips

INTRODUCTION

Echo-planar imaging (EPI) (1) is a rapid imaging technique, well suited for applications that require either high temporal resolution or short total acquisition times. A wide variety of applications take advantage of the speed performance of EPI, such as functional imaging (2), diffusion weighted imaging (3), perfusion imaging (4, 5), as well as interleaved EPI of the liver (6) and heart (7). An entire image usually can be acquired in times ranging from 50 to 200 ms.

Misregistrations of raw *k*-space data caused by system time delays and phase offsets are a significant problem for sequences such as EPI and gradient and spin-echo (8) where lines of *k*-space are acquired in two directions. System filters have causal impulse responses that manifest as *k*-space misregistrations (9, 10). Gradient hardware will also contribute to system delays, as will demodulators, RF coils, and other sources that are *patient independent*.

As described by several authors, "reference scans" are often used to measure time delays and phase offsets as part of the imaging protocol (10–12). Unfortunately, many reference techniques are object dependent, since the reference signal is modulated by field inhomogeneities and chemical shift. These effects can be reduced through the use of balanced reference scan techniques, however (12). Reference scans can add significant time to an MR examina-

tion, especially if the prescription plane is changing orientation and time delays are orientation dependent. This increases the total examination time and defeats the primary advantage of EPI: speed. Repeated reference scanning is not feasible with EPI based real-time MR systems, because scan planes are continually changing.

Cardiac imaging, in particular, poses several challenges for EPI. First, the field inhomogeneities present in the vicinity of the heart are accentuated by the proximity of the heart to the lungs in the mediastinum, as well as susceptibility effects from large veins carrying deoxygenated blood (13). In addition, ventricular motion and ventricular blood flow can cause significant phase shifts in the imaging signal. The geometry of the thorax itself can change between breath-holds, which may also present problems for EPI reference algorithms that are object dependent.

Once time delay estimates are made, postprocessing algorithms are often used to correct for these delays. These algorithms require additional computational expense that could be avoided by making delay corrections with gradient waveforms. In this way, the sampled data is free from timing misregistrations.

The following sections describe the effects of the anisotropic delays of gradients, and the time delay estimation bias and ghosting that results from this anisotropy is presented. "Compensation blips" are proposed and added to a pulse sequence to correct for anisotropic gradient delays in oblique coordinates. This eliminates the need for reference scans and postprocessing delay corrections. Examples of phantom and in vivo images using compensation blips are shown.

THEORY

Gradient hardware systems are the only orientation dependent source of system hardware delays. These delays can result from eddy currents (14), as well as sequencer errors that delay the intended waveform. Regardless of their source, these delays can be modeled as a time shift of the entire gradient waveform.

The incremental delay will be independent of slice orientation when the delay from each of the different gradient amplifier is the same. If these delays are different, however, the effective delay becomes image orientation dependent. Such anisotropy has serious implications for echo-planar image reconstruction, especially for real-time EPI systems that rapidly change image orientation and require rapid image reconstruction and delay compensation, without repeated reference scans.

Time shifts of gradient waveforms can only correct anisotropic delays to the precision of the gradient waveform sequencers. For example, if the sequencer precision is 4 μ s, then delay corrections can only be made to the nearest 2 μ s. At a bandwidth of ± 62.5 kHz, this represents a 0.25 sample shift, which can cause considerable ghosting (15).

¹Department of Biomedical Engineering, John Hopkins University School of Medicine, Baltimore, Maryland.

²Department of Radiology, John Hopkins University School of Medicine, Baltimore, Maryland.

Grant sponsor: National Institutes of Health; Grant number: HL45683; Grant sponsor: Whitaker Foundation; Grant sponsor: Medical Scientist Training Program. Elliot R. McVeigh is an Established Investigator of the American Heart Association.

*Correspondence to: Ergin Atalar, PhD., Department of Radiology, N. Caroline St., JHOC 4241, John Hopkins University School of Medicine, Baltimore, MD 21287-0845.

Received 16 September 1997; revised 8 June 1998; accepted 10 June 1998.

© 1999 Wiley-Liss, Inc.

The positions of the x, y, and z gradient coils determines the “physical coordinate system.” However, a coordinate system comprised of readout, phase encoding, and slice directions is called the “logical coordinate system.” A gradient waveform in logical coordinates is defined as $\underline{G}(t) = [G_r(t) \ G_p(t) \ G_s(t)]^T$ where $G_r(t)$, $G_p(t)$, and $G_s(t)$ represent the gradient waveforms in readout, phase, and slice encoding directions. The waveforms that are applied to each of the x, y, and z gradient amplifiers are calculated by a rotational transformation as: $\underline{G}'(t) = \mathbf{R}\underline{G}(t) = [G'_x(t) \ G'_y(t) \ G'_z(t)]^T$, where \mathbf{R} is the rotation matrix that maps the gradient waveforms from logical to physical coordinates. Figure 1 shows the three physical gradients of a readout gradient rotated to an arbitrary oblique orientation.

Next, consider a time delay operator that delays the physical gradient waveform, $\underline{G}'(t)$, in physical coordinates,

$$T[\underline{G}'] = T \begin{bmatrix} G'_x(t) \\ G'_y(t) \\ G'_z(t) \end{bmatrix} = \begin{bmatrix} G'_x(t - t_x) \\ G'_y(t - t_y) \\ G'_z(t - t_z) \end{bmatrix} \quad [1]$$

where t_x , t_y , and t_z are the delays for the x, y, and z gradients, respectively. Rotating $\underline{G}'(t)$ back into logical coordinates gives $\mathbf{R}^T T[\underline{G}']$, and calculating the k -space trajectory in logical coordinates,

$$\underline{k}(\tau) = \gamma \int_0^\tau \mathbf{R}^T T[\mathbf{R}[G_r(t) \ 0 \ 0]^T] dt = \gamma \mathbf{R}^T \int_0^\tau T[\mathbf{R}[G_r(t) \ 0 \ 0]^T] dt \quad [2]$$

assuming that $\underline{G}(t) = [G_r(t) \ 0 \ 0]^T$, which implies that the delays on the phase encoding blips do not contribute to delays in the readout direction. This assumption is valid as long as the phase encoding blips have been completed before data acquisition begins. In Fig. 2, the affect of the gradient delay on the k -space trajectory can be seen. For the trapezoid pulses shown in this figure, ramp time is $t_{\text{ramp}} = |G_r|/(dG_r/dt)$, where dG_r/dt is the slew rate of the gradient. Expansion of Eq. [2] gives

$$\underline{k}(\tau) = \gamma(\pm G_r) \begin{bmatrix} \tau - R_{11}^2 \left(t_x - \frac{t_x^2 (dG_r/dt)}{2G_r} \right) - R_{21}^2 \left(t_y - \frac{t_y^2 (dG_r/dt)}{2G_r} \right) - R_{31}^2 \left(t_z - \frac{t_z^2 (dG_r/dt)}{2G_r} \right) \\ \tau - R_{12}R_{11} \left(t_x - \frac{t_x^2 (dG_r/dt)}{2G_r} \right) - R_{22}R_{21} \left(t_y - \frac{t_y^2 (dG_r/dt)}{2G_r} \right) - R_{32}R_{31} \left(t_z - \frac{t_z^2 (dG_r/dt)}{2G_r} \right) \\ \tau - R_{13}R_{11} \left(t_x - \frac{t_x^2 (dG_r/dt)}{2G_r} \right) - R_{23}R_{21} \left(t_y - \frac{t_y^2 (dG_r/dt)}{2G_r} \right) - R_{33}R_{31} \left(t_z - \frac{t_z^2 (dG_r/dt)}{2G_r} \right) \end{bmatrix} \quad [3]$$

where R_{ij} is the rotation matrix element of the i th row and the j th column, and it has been assumed that the time delays are always shorter than ramp time t_{ramp} . It has been assumed that oblique rotation has not changed the readout gradient amplitude or effective slew rate, which may not be true for some oblique optimization procedures (16, 17).

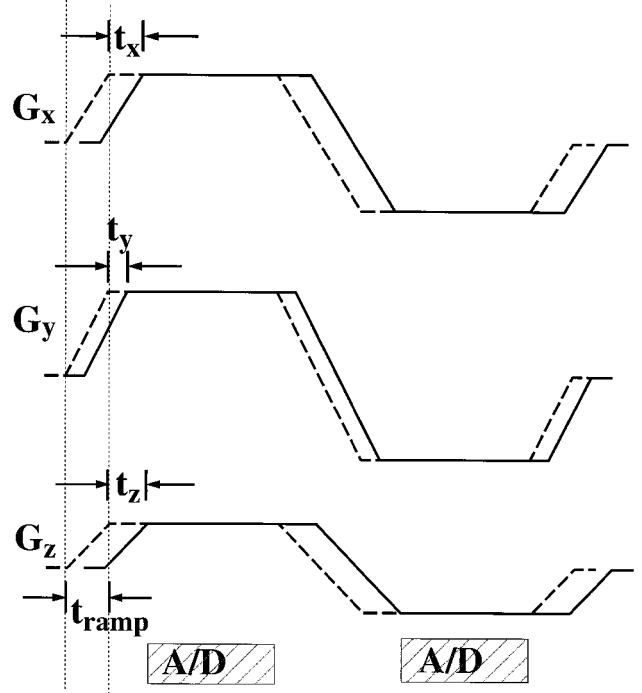


FIG. 1. Readout gradient after oblique rotation played on the three physical gradient axes. The time delays of the physical gradients (t_x , t_y , t_z), are shown, as well as the gradient ramp time (t_{ramp}). The sampling combs are also indicated (A/D).

The quadratic term $t_i^2(dG_r/dt)/2G_r$ ($i = x, y, z$) in Eq. [3] can be ignored,¹ allowing the shift in the readout direction to be written

$$\delta k_r = \pm \gamma G_r (R_{11}^2 t_x + R_{21}^2 t_y + R_{31}^2 t_z) \quad [4]$$

In the case that all delays are equal ($t_x = t_y = t_z$), then the effective shift in the readout direction is

$$\delta k_r = \pm \gamma G_r (R_{11}^2 + R_{21}^2 + R_{31}^2) t_x = \pm \gamma G_r t_x \quad [5]$$

independent of image orientation. However, if $t_x \neq t_y \neq t_z$

then the effective delay will be a weighted average of the individual delays.

As mentioned earlier, the total time delay is comprised of delays from the gradients as well as those from other sources, primarily the analog low-pass filter. Consider the

¹if $t_i = 3 \mu\text{s}$, $dG_r/dt = 120 \text{ (T/m)/s}$, $G_r = 2 \text{ G/cm}$, then $t_i^2(dG_r/dt)/2G_r = 0.027 \mu\text{s}$

delay measured in the i ($i = x, y$, or z) direction,

$$t_i = t_i^{\text{grad}} + t_{\text{filter}} \quad [6]$$

where t_i^{grad} is the delay contribution from the gradient only. Upon insertion into Eq. [4],

$$\delta k_r = \pm \gamma G_r (R_{11}^2 t_x^{\text{grad}} + R_{21}^2 t_y^{\text{grad}} + R_{31}^2 t_z^{\text{grad}} + t_{\text{filter}}) \quad [7]$$

showing that it is not necessary to separate the orientation dependent and independent components from one another.

Notice also from Eq. 3 that there are also effective shifts in the k_p and k_s directions. These shifts can be written

$$\delta k_p = \gamma (\pm G_r) (R_{12} R_{11} t_x + R_{22} R_{21} t_y + R_{32} R_{31} t_z) \quad [8]$$

and

$$\delta k_s = \gamma (\pm G_r) (R_{13} R_{11} t_x + R_{23} R_{21} t_y + R_{33} R_{31} t_z) \quad [9]$$

The shift in the phase encoding direction (δk_p) adds/subtracts additional phase encoding to even/odd echoes, and has been reported previously by Zhou et al. (18). This alternating shift in the phase encoding direction can cause ghosting artifacts (see Appendix).

This additional effective phase encoding can also bias delay calibration measurements. If anisotropic gradient delays are present and reference scans are made in oblique coordinates, the additional phase encoding caused by these delays will bias delay measurements made through reference scans. Since the additional phase encoding alternates between even and odd echoes, the bias it creates will not be removed by *any* reference method. Therefore, reference scans in oblique planes should be avoided. Correction for time delays in oblique image orientation can be made by measuring time delays in the three orthogonal axes and using Eq. [4] to calculate the effective delay in logical coordinates. This procedure is described below.

The shift in the slice direction (δk_s) will cause through slice dephasing. If the slice profile is asymmetrical, this dephasing will manifest as alternating phase shifts that will cause ghost artifacts, as previously described (15). If the slice profile is symmetric, it can be shown that this dephasing will only result in the loss of signal, without ghosting artifacts.

As an example of the magnitude of these shifts, consider an in-plane rotation of α degrees about the z axis. From Eq. [4], the shift in the readout direction becomes

$$\begin{aligned} \delta k_r &= \pm \gamma G_r (t_x \cos^2 \alpha + t_y \sin^2 \alpha) \\ &= \pm \gamma G_r \left(\left(\frac{t_x + t_y}{2} \right) + \left(\frac{t_x - t_y}{2} \right) \cos 2\alpha \right) \end{aligned} \quad [10]$$

The alternating phase encoding shift will be

$$\delta k_p = \pm \gamma G_r \left(\frac{t_y - t_x}{2} \right) \sin 2\alpha \quad [11]$$

and there is no additional encoding in the slice direction ($\delta k_s = 0$) in this case. Equations 10 and 11 explicitly show that *differences* in gradient delays are responsible for the orientation dependence of k -space misregistrations.

Figure 2 (a) depicts the k -space trajectory after an in-plane rotation when $t_x > t_y$. Notice the shift in the phase encoding direction, δk_p , even though no phase encoding pulse was played. As well, the second echo is phase encoded in the *opposite* direction, by an amount $-\delta k_p$. The numbers in this figure correspond to those shown with the physical gradient waveforms in Fig. 2 (b).

In the worst case, set $\alpha = 45^\circ$. For a 32-cm FOV and ± 64 kHz bandwidth, G_r will be 0.92 G/cm and Δk_p will be 0.20 cm^{-1} . If it is assumed that the differential gradient time delay ($t_x - t_y$) is 2 μs then $\delta k_p = \pm 0.025$ cm^{-1} , about $1/8$ of Δk_p . This is a substantial shift that will cause ghost artifacts, as described in the Appendix. These artifacts are difficult to correct with postprocessing algorithms.

Ghosting artifacts in the readout direction will also be present, although these delays can be corrected with reference scans and postprocessing delay corrections. The

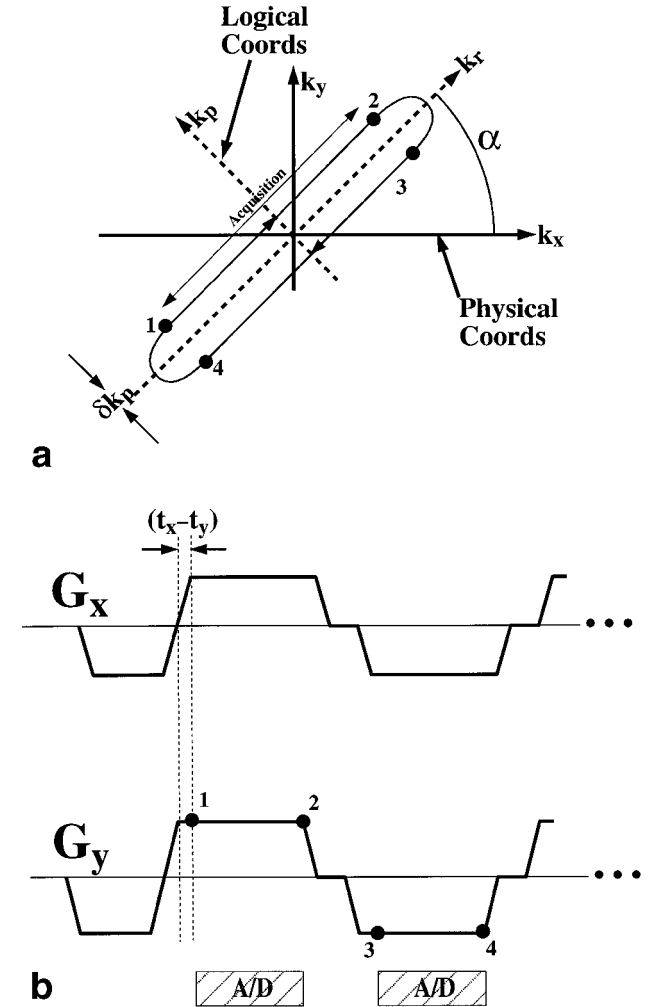


FIG. 2. (a) k -space trajectory after an in-plane rotation, for the physical gradient with anisotropic delays, shown in (b). The numbers in (b) correspond to the positions in k -space shown in (a). The sampling combs are also indicated (A/D). The shift in the readout direction is not depicted in these figures.

effective readout delay is orientation dependent, however, and will require new reference scan measurements as the orientation changes.

Image orientation dependent k -space shifts (δk_r , δk_p , δk_s) are easily calculated with knowledge of the three delays of the physical gradients (t_x , t_y , t_z), and the rotation matrix \mathbf{R} . With this information, delay corrections and encoding corrections can be made by modifying the *pulse sequence* itself with “compensation blips,” as described below.

METHODS

Scanner Calibration Algorithm

Calibration of a scanner requires that delays in the three orthogonal directions be measured. The following algorithm outlines a methodology for calibrating a scanner using a phantom:

for each orthogonal axis (x , y , z)

for both readout gradient polarities (\pm)

- Acquire echo train without phase encoding blips
- Fourier transform each echo

for each echo pair

- Regress phase difference of complex profiles to estimate delays using the balanced reference method recently reported (12)

This requires a total of six excitations for each filter setting, a calibration procedure that is relatively simple and fast. If the contribution to the delay from different filters is known, then this component can be subtracted, reducing the total number of delay measurements to three for complete scanner delay calibration.

A primary advantage of scanner calibration is that time is not required during a patient study for reference scans. Furthermore, multiple averaging can be performed with calibration scans to ensure highly accurate estimates of time delays. This greatly reduces the ghost to noise ratio of residual ghosting caused by time delays and constant phase shifts (15).

Correction for System Delays and Phase Offsets

Many EPI systems rely on postprocessing routines to correct for time delays and constant phase offsets. This is usually done by applying the principles of the Fourier shift theorem. After Fourier transformation in the read-out direction, each profile is multiplied by the appropriate phase roll and constant phase offset, before Fourier transformation in the phase encoding direction. Although such postprocessing algorithms can be effective and accurate only when the gradient waveform delays are isotropic, a more attractive and computationally less expensive approach would be to modify the gradient waveform to produce data that does not require correction even with anisotropic gradient waveform delays.

Once time delay calibration of a scanner has been performed, there are several steps that can be taken to correct for the system hardware delays. The easiest way to correct for orientation independent delays from within the pulse sequence is to delay the sampling period to better align echoes in the readout direction of k -space. As well, anisotropic gradient delays can be compensated by shifting entire *physical* gradient waveforms by $-t_x$, $-t_y$, and $-t_z$ for

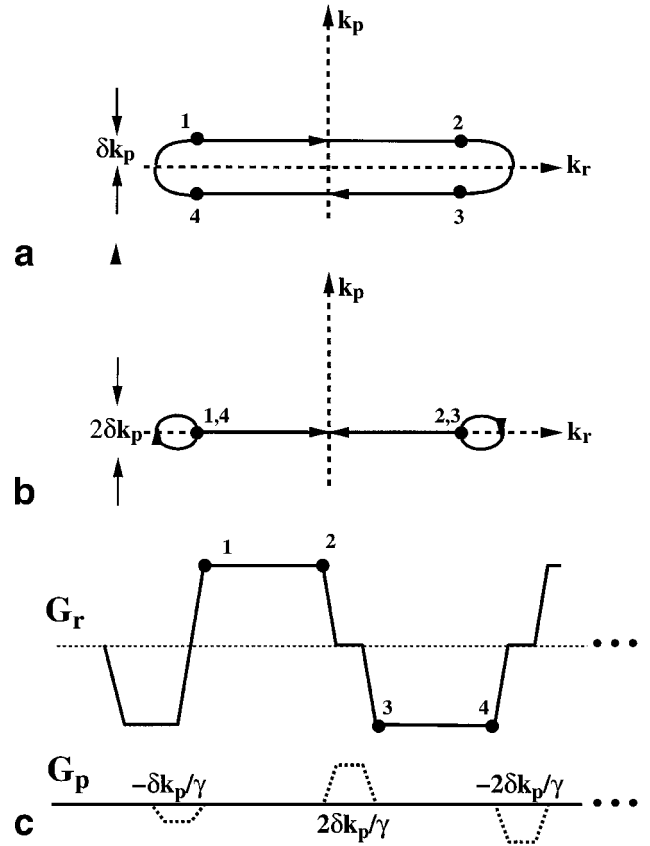


FIG. 3. (a) Logical k -space trajectory for two echoes without phase encoding direction compensation blips (phase encoding blips off). (b) Compensated k -space trajectory using the sequence shown in (c). This removes the alternating shift ($\pm\delta k_p$) resulting from anisotropic gradient delays. Numbers in (a) and (b) correspond to the position in k -space shown in (c). The area under the first blip is $-\delta k_p/\gamma$ and $\pm 2\delta k_p/\gamma$ for subsequent blips. Compensation blips are not drawn to scale.

the x , y , and z physical gradients. This latter correction is only possible, however, in pulse sequences that calculate and play *physical* waveforms, and do not rely upon oblique rotation boards. In any case, simple shifts of the gradient waveforms and sampling periods can only correct delays to the precision of the gradient waveform sequencers.

Although the residual delay can be removed with the postprocessing algorithms, an alternative is to use “compensation blips” to adjust the position of the echoes in the readout direction. This can be done very accurately, since the area of a gradient blip can be adjusted with high precision. As well, the additional encoding in the phase encoding and slice directions caused by anisotropic gradient delays is difficult to remove by postprocessing. Zhou et al. (18) have previously suggested compensation blips for removal of the additional encoding in the phase encoding direction. Such blips can also be used to compensate for k -space misregistrations in the readout and slice directions, caused by gradient delay anisotropy. As is described in detail below, compensation blips are programmed in logical coordinates, allowing pulse sequences programmed in logical coordinates to make delay corrections with simple modifications to the gradient waveforms.

Lastly, constant phase offsets are easily removed by adjusting the phase of the system receiver. Since this phase

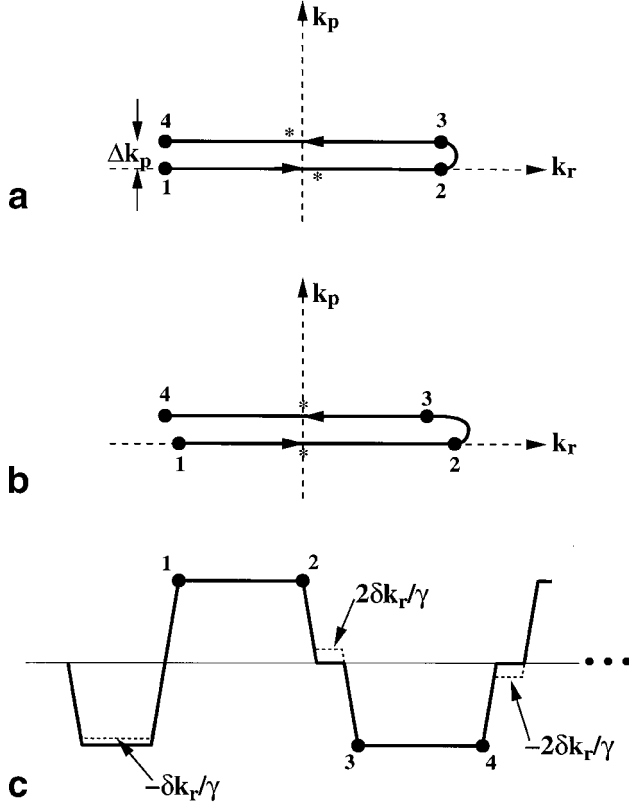


FIG. 4. (a) Logical k -space trajectory for two echoes without readout direction compensation blips. Misregistrations in the phase encoding direction ($\pm\delta k_p$) have been ignored and a phase encoding blip has been played (not shown) to advance the position in k -space by Δk_p . Asterisks (*) denote the position of echo within the data matrix. (b) Compensated k -space trajectory using the sequence shown in (c). This removes the alternating shift in the logical readout direction ($\pm\delta k_r$) resulting from anisotropic gradient delays. Numbers in (b) correspond to the position in k -space also shown in (c). The area under the first blip is $-\delta k_r/\gamma$ and $\pm 2\delta k_r/\gamma$ for subsequent blips. Compensation blips are not drawn to scale.

can be adjusted with high precision, accurate correction of constant phase offsets between even and odd echoes is easily attained and need not rely on postprocessing corrections.

Compensation Blips

Correction for anisotropic gradient delays through time shifts can only be made within the precision of the gradient waveforms, usually a few microseconds; simple time shifts in the gradient waveforms cannot correct for anisotropic time delays. As well, time shifts in the gradient waveforms are difficult to implement in sequences that are programmed in logical coordinates and rely on oblique rotation boards to execute gradient waveforms in physical coordinates. *Compensation blips*, however, can correct for the effects of anisotropic gradient delays by compensating for orientation dependent k -space misalignments. Corrections can be made in the readout, phase encoding, and slice directions by adding the appropriate blips to the *logical* sequence.

Compensation blips for correction of additional phase encoding are depicted in Fig. 3. In this diagram, the logical k -space trajectory for two consecutive echoes is shown in

Fig. 3 (a) with no compensation (phase encoding off). Figure 3 (b) shows the compensated trajectory using the compensation blips diagrammed in Fig. 3 (c). The numbers in Fig. 3 (c) correspond to the positions in k -space shown in Fig. 3 (a) and 3 (b). The first compensation blip has area $-\delta k_p/\gamma$, and the following blips have area $\pm 2\delta k_p/\gamma$, as shown, for subsequent echoes. In practice, these blips are added to the standard phase encoding blips, which have considerably larger area than the compensation blips.

Misregistrations in the readout direction can also be corrected using compensation blips, by adjusting the position in k -space as the k_r sampling moves back and forth. Figure 4 demonstrates the use of compensation blips to correct for echo shifting in the readout direction. This is achieved by ensuring that the area of the readout prephaser is increased by $-\delta k_r/\gamma$, and the net area of the readout gradient between plateaus is $\pm 2\delta k_r/\gamma$, as diagrammed in Fig. 4.

Although not shown, compensation blips can also be introduced on the slice select axis to unwind the alternating dephasing of the slice. In general, compensation blips require little to no additional time to execute, and only require knowledge of the rotation matrix, \mathbf{R} , and the three physical gradient delays (t_x , t_y , t_z).

Time Delay Compensation Algorithm

During image acquisition, the following procedure is followed to remove system time delays and constant phase offsets by modification of the pulse sequence.

1. The sampling period and physical gradients are shifted in time to make corrections for filter delays and anisotropic gradient delays.
2. The residual delays for each physical gradient t'_x , t'_y , and t'_z , and the rotation matrix \mathbf{R} are used to calculate

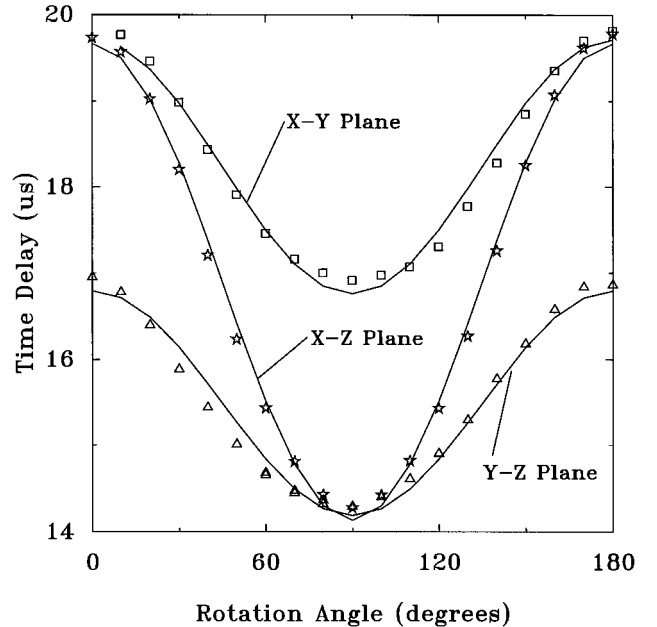


FIG. 5. Time delays measured for reference scans at different orientations, rotated in the X-Y, X-Z, and Y-Z planes. Symbols represent measured data, and solid lines are curves fit to Eq. [10]. The fit values for the three times delays were: $t_x = 19.7 \mu\text{s}$, $t_y = 16.8 \mu\text{s}$, and $t_z = 14.2 \mu\text{s}$.

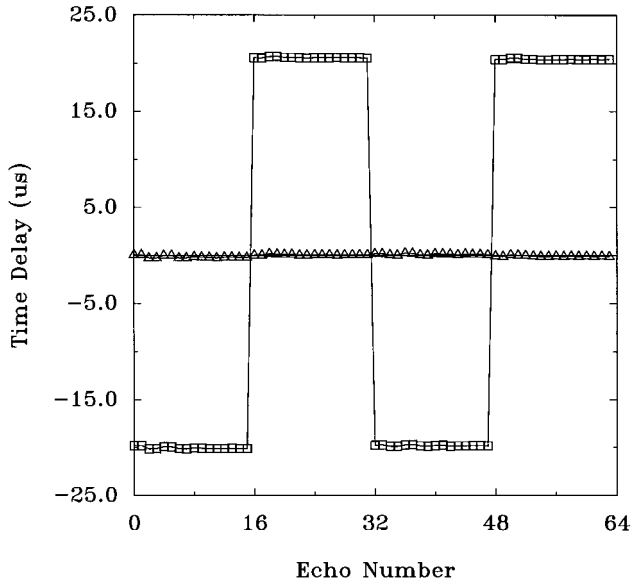


FIG. 6. Time delays (μs) plotted against phase encoding index for a four-echo train length EPI data set before and after compensation blip correction. Accurate correction of the delay is seen.

compensation blips for slice, readout, and phase encoding gradients.

3. The phase of the receiver is adjusted to compensate for constant phase offsets between even and odd echoes.
4. The compensated image is acquired and reconstructed without special postprocessing corrections for delays.

The final result should be an image free from ghosting artifacts caused by system time delays.

Imaging

All experiments were performed on a GE Signa 1.5 T Horizon (version 5.5). This scanner has shielded gradients with maximum gradient strength of 2.2 G/cm and slew rate of 120 (T/m)/s on all three axes.

Compensation blips were added to a recently developed multiecho spoiled gradient echo sequence (19). This sequence uses hardware optimized trapezoid (HOT) gradient waveforms to minimize dead period durations (16). The HOT algorithm minimizes TR and TE, and maximizes sequence efficiency for a given oblique orientation. Manufac-

turer interleaved EPI sequences also were used to make scanner delay measurements, shown in the following sections.

RESULTS

Time Delays Measured in Oblique Orientations

Figure 5 plots the measured delays (symbols) in the X-Y, X-Z, and Y-Z planes, against the rotation angle in that plane, using the balanced reference scan recently reported (12). The solid lines are plots of Eq. [10], fit to determine the best estimate of t_x , t_y , and t_z , equal to 19.7 μs , 16.8 μs , and 14.2 μs , respectively. As seen in this figure, Eq. [10] accurately describes the behavior of the measured time delays as the readout direction is rotated obliquely.

It should be noted that no corrections were made to remove bias caused by shifts in the phase encoding direction on the time delay measurements in oblique orientations shown in Fig. 5. The strong orientation dependence of time delays with orientation is apparent, even in the presence of any potential bias.

Compensation Blip Correction

Figure 6 plots the time delays measured from two raw data sets, before and after readout compensation blips were used to correct these delays. Accurate compensation of these delays is apparent from this figure, demonstrating the effectiveness of compensation blips in the readout direction.

Figure 7 contains single shot axial images of a water phantom, with and without compensation blips. In the first image, no compensation was used. In the second and third images, only readout and phase encoding compensation blips were used, respectively, whereas the fourth has both. This figure shows that compensation blips in both the readout and phase encoding directions are necessary to eliminate ghosting artifacts. No postprocessing corrections were made.

Figure 8 shows two shot echo-planar brain images acquired with (Fig. 8 (a)) and without (Fig. 8 (b)) compensation blips to correct for system time delays. A chemical saturation pulse was used to minimize artifacts from fat. Compensation blips have removed ghosting artifacts without any postprocessing.

DISCUSSION

In this work, new strategies for the correction of time delays in echo-planar imaging have been described.

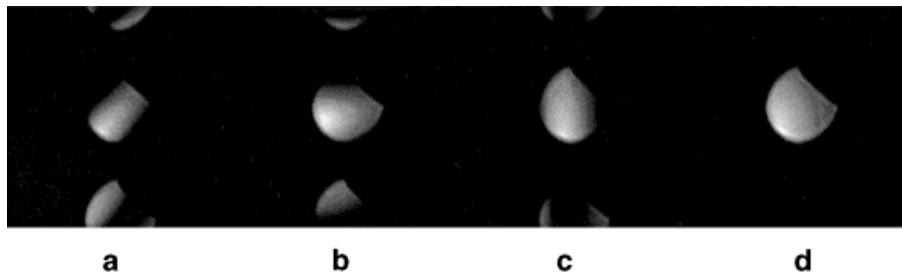


FIG. 7. Axial single shot images of a water phantom, after 45° in-plane rotation, (a) without any compensation, (b) with compensation in the logical readout direction only, (c) in the logical phase encoding direction only, and (d) compensation in both directions. Other imaging parameters include: 128 × 128 matrix, 90° flip angle, 32-cm FOV, 8-mm slice thickness, and ± 64 kHz. Phase encoding is in the vertical direction.

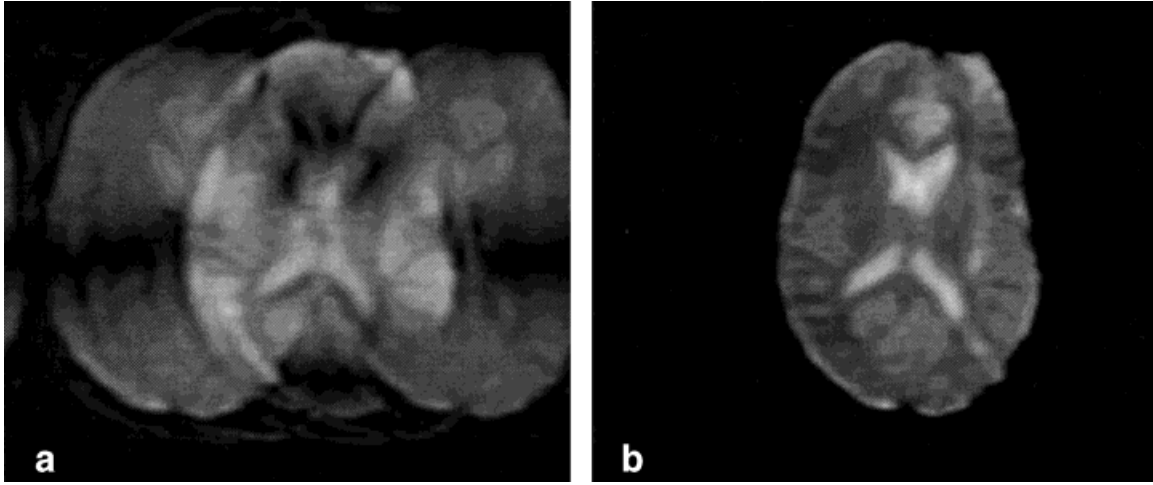


FIG. 8. Two-shot axial echo-planar image of a brain, (a) before, and (b) after compensation blip correction. Other imaging parameters include: 160×80 matrix, 90° flip angle, 28-cm FOV, 8-mm slice thickness, and chemical presaturation was used to reduce fat artifacts. Phase encoding is in the horizontal direction.

The effects of anisotropic gradient delays were investigated and it was shown, and verified experimentally, that total system delays measured in oblique coordinates are dependent on image orientation. It was also shown that these delays can be easily predicted, knowing the rotation matrix for that orientation and the delays of the three orthogonal directions.

Anisotropic delays were also shown to cause a new form of ghosting artifact resulting from alternating k -space shifts in the phase encoding direction. In the Appendix, analytical expressions describing this artifact are presented.

Shifts in k -space caused by anisotropic delays will bias time delay measurements made with reference scans in oblique coordinates. For this reason, EPI techniques that rely on reference scan measurements should avoid these measurements in oblique coordinates. Instead, individual reference measurements in the three orthogonal axes should be performed, followed by appropriate rotation of the delays as described in this work.

A calibration algorithm was discussed, using a balanced reference estimator to measure delays in the three orthogonal directions. Once a scanner has been calibrated for

anisotropic time delays, compensation blips were shown to be an effective means of removing these delays, without the need for postprocessing corrections. This has important implications for real-time EPI applications that require rapid changes in scan plane positioning and should avoid repeated reference measurements and postprocessing.

APPENDIX

Ghosting Artifacts from Oblique Imaging

There are three sources of ghosting that arise from oblique imaging with anisotropic gradient delays. First, the effective time delay has been shown to be dependent on the imaging orientation, and proper correction must be used to compensate for these delays in the readout direction. The next source of ghosting can result from the alternating encoding in the slice direction. At worst, this results in an alternating phase shift and will cause ghosts as previously described (15). The last source of ghosting results from additional alternating phase encoding caused by anisotropic gradient delays, and is described below.

Consider a one-dimensional profile $s(k_p)$ in the phase encoding direction, discretized at intervals Δk_p , such that $s[k] = s(k\Delta k_p)$. A profile that was phase encoded by an additional amount $\pm\delta k_p$ would take the form $s[k \mp \tilde{k}] = s(k\Delta k_p \mp \delta k_p)$, where $\tilde{k} = \delta k_p / \Delta k_p$ represents the sample shift in the phase encoding direction. This shifting effect is shown schematically in Fig. 9. Thus, the profile in the phase encoding direction of a raw discretized EPI k -space matrix can be written

$$s'[k] = s[k - \tilde{k}]g[k] + s[k + \tilde{k}]g[k - n_l] \quad [A1]$$

where $g[k]$ is defined as

$$g[k] = \begin{cases} 1 & \text{if } 2l n_l \leq k \leq (2l + 1)n_l \\ 0 & \text{otherwise for any integer } l \end{cases} \quad [A2]$$

where n_l is the number of interleaves. This function has been described previously (15) in the description of ghost-

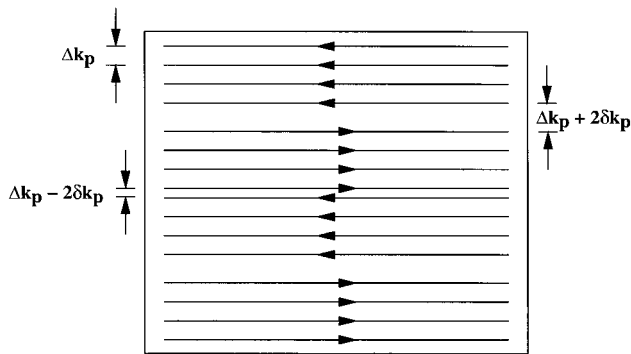


FIG. 9. Phase encoding shifts in the oblique EPI data matrix resulting from anisotropic gradient time delays. The shift δk_p , as well as the separation between lines of k -space, Δk_p are indicated. In this example, $n_l = 4$ and $N_p = 16$, and arrows indicate even and odd echoes.

ing artifacts. Taking the N_p -point discrete Fourier transform (DFT) of Eq. [A1] gives

$$S'[n_p] = (S[n_p]e^{-j2\pi\tilde{k}n_p/N_p}) *_c G[n_p] + (S[n_p]e^{j2\pi\tilde{k}n_p/N_p}) *_c (G[n_p]e^{-j2\pi n_p n_p/N_p}) \quad [A3]$$

where $G[n_p]$ is the DFT of $g[k]$ and $*_c$ is the circular convolution operator. Rearranging

$$S'[n_p] = \left(S[n_p] \cos\left(\frac{2\pi\tilde{k}n_p}{N_p}\right) \right) *_c (N_p\delta[n_p]) + \left(jS[n_p] \sin\left(\frac{2\pi\tilde{k}n_p}{N_p}\right) \right) *_c (G[n_p]e^{-j2\pi n_p n_p/N_p} - G[n_p]) \quad [A4]$$

Eq. [A4] can be written

$$S'[n_p] = I[n_p] + H[n_p] \quad [A5]$$

where $I[n_p]$ is the central image, which has been attenuated by an amount $\cos 2\pi\tilde{k}n_p/N_p$,

$$I[n_p] = \left(S[n_p] \cos\left(\frac{2\pi\tilde{k}n_p}{N_p}\right) \right) *_c (N_p\delta[n_p]) \quad [A6]$$

and $H[n_p]$ is the ghost artifact. Solving for $G[n_p]$ (15), $H[n_p]$ becomes

$$H[n_p] = \left(S[n_p] \sin\left(\frac{2\pi\tilde{k}n_p}{N_p}\right) \right) *_c \left(\frac{N_p}{n_i} (-1)^n e^{-j\pi(2n_i-1)n_p/N_p} \frac{\sin^2\left(\frac{\pi n_i n_p}{N_p}\right)}{\sin\left(\frac{\pi n_i}{N_p}\right)} \times \sum_{m=-n_i}^{n_i-1} \delta\left[n_p - \frac{N_p m}{2n_i}\right] \right), m \text{ odd} \quad [A7]$$

The separation between ghosts is N_p/n_i pixels, and the most intense ghosts are those closest to the central image are the $m = \pm 1$ ghosts. As an estimate of ghost intensity, take $m = 1$, normalize by the image intensity free of artifacts (N_p), and ignore all phase terms,

$$|H[n_p]| = \frac{1}{n_i \sin \frac{\pi}{2n_i}} \left(S[n_p] \sin\left(\frac{2\pi\tilde{k}n_p}{N_p}\right) \right) *_c \delta\left[n_p - \frac{N_p}{2n_i}\right] \quad [A8]$$

As a test object, take

$$S[n_p] = \text{rect}\left(\frac{n_p}{\eta N_p}\right)$$

where η is the fraction of the field of view that this rectangular object occupies. For $\tilde{k} \leq 0.5$, the ghost intensity

is highest at the edge of the object, where $n_p = \eta N_p/2$,

$$\left| H\left[\frac{\eta N_p}{2}\right] \right| = \frac{\sin(\pi\tilde{k}\eta)}{n_i \sin\left(\frac{\pi}{2n_i}\right)} \quad [A9]$$

representing the maximum ghosting intensity for an n_i interleaved EPI data matrix and an alternating phase encoding shift of $\delta k_p = k\Delta k_p$. As an example, let $\eta = 0.5$, $n_i = 1$, $\alpha = 45^\circ$, FOV = 32 cm, bandwidth = ± 64 kHz, and let the time delay be 2 μ s. For these parameters, $G_r = 0.92$ G/cm, $\Delta K_p = 0.20$ cm $^{-1}$, $\delta k_p = \pm 0.025$ cm $^{-1}$, and $|H[\eta N_p/2]| = 0.20$. This is a significant fraction (20%) of the ghost free image intensity.

ACKNOWLEDGMENTS

The authors gratefully acknowledge helpful discussions with Bradley Bolster, MSE.

REFERENCES

- Mansfield P. Multi-planar image formation using NMR spin-echoes. J Phys C 1977; 10:L55–L58.
- Kwong KK. Functional magnetic resonance imaging with echo planar imaging. Magn Reson Q 1995; 11:1–20.
- Turner R, LeBihan D. Single-shot diffusion imaging at 2.0 Tesla. J Magn Reson Imaging 1990; 86:445–452.
- Moseley ME, Sevic R, Wendland MF, White DL, Mintonovitch J, Asgari HS, Kucharczyk J. Ultrafast magnetic resonance imaging: diffusion and perfusion. Can Assoc Radiol J 1991; 42:31–38.
- Stehling MK, Turner R, Mansfield P. Echo-planar imaging: magnetic resonance imaging in a fraction of a second. Science 1991; 254:43–50.
- Butts K, Riederer SJ, Ehman RL, Felmlee JP, Grimm RC. Echo-planar imaging of the liver with a standard MR imaging system. Radiology 1993; 189:259–264.
- McKinnon GC. Ultrafast interleaved gradient-echo-planar imaging on a standard scanner. Magn Reson Med 1993; 30:609–616.
- Oshio K, Feinberg DA. GRASE (gradient- and spin-echo) imaging: a novel fast MRI technique. Magn Reson Med 1991; 20:344–349.
- Oppenheim AV, Shafer RW. Discrete Time Signal Processing. Prentice Hall, 1982.
- Bruder H, Fischer H, Reinfelder HE, Schmitt F. Image reconstruction for echo planar imaging with non-equidistant k-space sampling. Magn Reson Med 1992; 23:311–323.
- Jesmanowicz A, Wong EC, Hyde JS. Phase correction for EPI using internal reference lines. In "Proc., SMRM, 12th Annual Meeting, New York, 1993," p. 1239.
- Reeder SB, Atalar E, McVeigh ER. Echo delay estimation in echo planar reference scans: implications for artifact reduction. In "Proc., ISMRM, 4th Annual Meeting, New York, 1996," p. 1479.
- Reeder SB, Faranesh AZ, Boxerman JL, McVeigh ER. In vivo measurement of T_2^* in human hearts at 1.5T: implications for cardiac echo planar imaging. Magn Reson Med 1998; 39:988–998.
- Ahn CB, Cho ZH. Analysis of eddy currents in nuclear magnetic resonance imaging. Magn Reson Med 1991; 17:149–163.
- Reeder SB, Atalar E, Bolster BD, McVeigh ER. Quantification and reduction of ghosting artifacts in interleaved echo planar imaging. Magn Reson Med 1997; 38:429–439.
- Atalar E, McVeigh ER. Minimization of dead-periods in MRI pulse sequences for imaging oblique planes. Magn Reson Med 1994; 32:773–777.
- Bernstein MA, Licato PE. Angle-dependent utilization of gradient hardware for oblique MR imaging. J Magn Reson Imaging 1994; 4:105–108.
- Zhou X, Epstein FH, Maier JK. Reduction of a new nyquist ghost in oblique echo planar imaging. Proc., ISMRM 4th Annual Meeting, New York, 1996, p. 1477.
- Reeder SB, Atalar E, Faranesh AZ, McVeigh ER. Multi-echo segmented k-space imaging: a hybrid sequence for ultra-fast cardiac imaging. Magn Reson Med, in press.